

Recombination dynamics in low-dimensional nitride semiconductors

Y. Kawakami^{*1}, A. Kaneta¹, K. Omae^{**1}, A. Shikanai¹, K. Okamoto^{***1}, G. Marutsuki²,
Y. Narukawa², T. Mukai², and Sg. Fujita¹

¹ Department of Electronic Science and Engineering, Kyoto University, Kyoto 606-8501, Japan

² Nichia Corporation, 491 Oka, Kaminaka, Anan, Tokushima, 774-8601 Japan

Received 14 April 2003, revised 3 June 2003, accepted 7 August 2003

Published online 7 November 2003

PACS 68.37.Uv, 78.47.+p

Optical properties induced by two major effects, potential fluctuation and piezoelectric fields, have been assessed to interpret the emission mechanism in low-dimensional nitride semiconductors because the former leads to the exciton/carrier localization, and the latter to the quantum confined Stark effect (QCSE). Degenerated white-light pump-and-probe spectroscopy has been employed to assess which factor plays an important role in the series of $\text{In}_x\text{Ga}_{1-x}\text{N}$ multiple quantum well (MQW) structures whose well widths are 3 nm, 5 nm and 10 nm. Moreover, photoluminescence (PL) mapping with scanning near-field optical microscopy (SNOM) has revealed the dense distribution of island-like structures, the size of which ranges from 20 nm to 70 nm in a 3 nm-thick $\text{In}_x\text{Ga}_{1-x}\text{N}$ single quantum well (SQW) structure emitting at blue spectral region.

© 2003 WILEY-VCH Verlag GmbH & Co. KGaA, Weinheim

1 Introduction Recent developments in the growth technology of $\text{In}_x\text{Ga}_{1-x}\text{N}/\text{GaN}/\text{Al}_y\text{Ga}_{1-y}\text{N}$ heterostructures have led to the realization of incandescent violet, blue, green and amber light emitting diodes (LEDs) [1, 2], as well as of laser diodes (LDs) [3, 4] operated from ultraviolet (366 nm) to blue (480 nm) spectral region. The reason why the tuning range of LDs for cw operation is much narrower than that of LEDs is probably because of two reasons. The first one is the effect of piezo-electric field. The most devices are grown toward c-direction with hexagonal structures, so that large internal electric field is induced to the growth direction. This electric field is in the order of MV/cm, so the optical dipole, as well as transition energies is reduced due to the separation between electron and hole wavefunctions. Such effects are called as Franz–Keldysh effect and quantum confined Stark effect (QCSE). The second one is potential fluctuation induced by inhomogeneity of both In compositions and well widths. This limits the number of density of states due to the formation of localized tail states. Because of these effects, large Stokes shift between absorption and emission is observed, as well as significant blue shift of emission energy with increasing injected-carrier density. The problem is that it is very difficult to know with conventional optical measurement which factor limits the recombination mechanism because both two effects can contribute to observed phenomena. It should be noted here that the major factor changes with the sample, because the effect of internal electric field is enhanced with increasing well width, and is reduced with increasing background doping concentration and with carrier injection, and also the degree of potential fluctuation is changed with the difference in growth conditions. Therefore, the precise optical characterization is needed in each sample to determine the recombination mechanism.

* Corresponding author: e-mail: kawakami@kuee.kyoto-u.ac.jp, Phone: +81 75 753 5295, Fax: +81 75 753 5898

** Present address: Department of Electrical Engineering, Osaka University, 2-1 Yamadaoka Suita, Osaka 565-0871, Japan

*** Present address: Department of Electrical Engineering, California Institute of Technology, Pasadena, CA 91125, USA

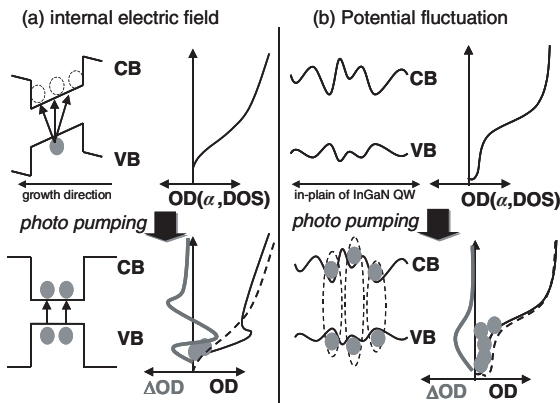


Fig. 1 Schematic of band structures, as well as OD and ΔOD spectra in InGaN quantum wells under a) internal electric field and b) potential fluctuation.

Two effects, internal electric fields versus potential fluctuation can be separated if the photo-induced change of absorption spectra is characterized as shown in Fig. 1. Both effects contribute to the broadening of absorption edge, for (a) due to Franz–Keldysh and QCSE effects, and (b) due to the formation of localized tail states. So, it is difficult to separate two effects by linear absorption spectra. However, the modification of such optical density due to injected carriers is different between two cases. In case of (a), internal electric field is reduced by the screening effect, so the optical density (OD) spectra corresponding to absorption spectra (as well as to density of states [DOS]) become sharp, so the feature of photo-induced change of OD (ΔOD) is as shown in the figure, where the positive signal is sandwiched between two negative signals [5]. However, in case of (b), only the negative signal is observed in ΔOD due to the band-filling of localized-tail states. Motivated by this idea, the dynamics of ΔOD was estimated by employing white-light pump-and-probe spectroscopy to $\text{In}_x\text{Ga}_{1-x}\text{N}/\text{GaN}$ multiple quantum well (MQW) structures [6, 7].

Despite high threading-dislocation density (10^8 – 10^{10} cm^{-2}) in $\text{In}_x\text{Ga}_{1-x}\text{N}$ -based epilayers grown on sapphire substrates fabricated LEDs show substantially high external quantum efficiency (η_{ext}). The η_{ext} is particularly high in the wavelength from 380 to 490 nm, so that $\eta_{\text{ext}} = \text{about } 20\%$ is now commercially available, and $\eta_{\text{ext}} = \text{about } 40\%$ is achieved experimentally in LEDs operated at violet to blue spectral range. Two models have been reported so far to account for such phenomena correlating to recombination dynamics. The first one is that incorporation of In to Ga-site is effective for suppressing nonradiative recombination centers related to point defects [8]. Another one is the effect of exciton localization induced by compositional fluctuation of In, where the pathways of nonradiative recombination centers are hindered once excitons are captured at potential minima [9–11]. Nevertheless, it is very important for the further improvement in emission efficiency to correlate radiative/nonradiative recombination processes with micro/nanoscale structures as shown in Fig. 2, and to make a positive-feedback to the design and the fabrication conditions of GaN-based LEDs. As for the assessment of potential fluctuation, a number of reports have recently been appeared on the spatial mapping of luminescence in $\text{In}_x\text{Ga}_{1-x}\text{N}$ single-

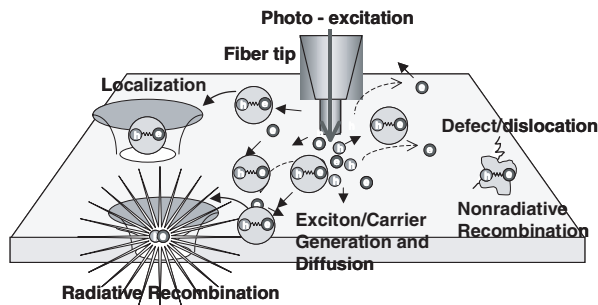


Fig. 2 Schematic of exciton/carrier generation induced by local photoexcitation by fiber tip, and of diffusion, localization, radiative and nonradiative recombination processes in semiconductors.

quantum-wells (SQWs) by cathodoluminescence (CL), [12–14] or by photoluminescence (PL) using scanning-near field optical microscopy (SNOM) [15–18]. Vertikov et al. performed the SNOM-PL mapping in thin $\text{In}_x\text{Ga}_{1-x}\text{N}/\text{GaN}$ epilayers and QWs with the spatial resolution of 100 nm [16].

The most of SNOM results were obtained using home-built illumination-mode system, where the laser light was focused into a few hundred nm^2 spot through the SNOM tip composed of tapered optical fiber and the PL spectra were probed by objective lens. A drawback of such a system is that it is very difficult to know whether excitons and/or carriers producing PL are directly photo-generated at the probe region or they are diffused out from it. This problem can be overcome by means of illumination-collection mode [19] developed recently for the assessment of widegap semiconductors [17, 18], where photo-excitation and the PL probing are performed using the same fiber tip because the spatial resolution is solely limited by the diameter of aperture formed at the tip of fiber probe. In this paper, we developed the SNOM technique to characterize the micro/nanoscale optical properties in nitride-based semiconductors. Time-resolved SNOM-PL results taken at an $\text{In}_x\text{Ga}_{1-x}\text{N}$ -SQW structure revealed the critical evidence that supports the model of diffusion of excitons to potential minima.

2 Experimental procedure The pump beam for pump-and-probe spectroscopy (wavelength; 370 nm, pulse width; 150 fs and repetition rate; 1 kHz) was formed by passing the output beam from regenerative amplifier (RGA) to optical parametric amplifier (OPA). The white-light probe beam was generated by focusing the part of output beam from RGA on a D_2O cell. The delay time of the probe beam with respect to the pump beam was tuned by changing the position of the retroreflector controlled by the pulse stage. In order to detect the probe beam with spatially uniform carrier distribution in the sample, the focus diameter of the pump beam (500 μm) was set substantially larger than that of the probe beam (100 μm). Moreover, the probe beam was perpendicularly polarized with respect to the pump beam, and the transmitted probe beam from the sample polarized in this direction was detected to avoid the detection of the scattered component of the pump beam. Both pump and probe beams were detected by a dual photo-diode array in conjunction with a 25 cm monochromator. The whole measurement was done at 10 K.

The SNOM measurements were performed with NFS-300 near-field spectrometer developed at JASCO Corp. that is capable of PL mapping with optical fiber tips under both an illumination collection mode and an illumination mode. Double-tapered Ge-doped- SiO_2 fibers with aperture diameter of 30 nm were used as probing tips. The sample-probe separation was controlled by detecting the amplitude of dithered probe. The amplitude of this oscillation was less than 1 nm at the first-order resonance frequency of the probe, and was fed back to control the height of the sample PZT ($\text{Pb}(\text{Zr}, \text{Ti})\text{O}_3$) stage. As a result, the sample-probe separation was regulated to be 10 nm. The cooling of the samples was performed by flowing cool He gas. The stable measurement was achieved by flowing an appropriated flux of He gas from the bottom to the top parts of the cryostat. An $\text{In}_x\text{Ga}_{1-x}\text{N}$ -based laser diode emitting at 400 nm (developed at Nichia Corp.) was used as the excitation source. An optical power of 1 mW was coupled to the probe, and about 0.1 μW was used to illuminate the samples through the probe. PL signal was collected by the probe, and was introduced into a monochromator in conjunction with a cooled charge-coupled device (CCD) detector (Roper Scientific, Spec-10: 400B/LN).

3 Result and discussion Three types of samples were prepared for the pump-and-probe spectroscopy. Their active layers consist of a 10 nm/10 nm thick $\text{In}_{0.1}\text{Ga}_{0.9}\text{N}$ MQW with 3 period [sample (a)], a 5 nm/10 nm thick $\text{In}_{0.1}\text{Ga}_{0.9}\text{N}$ MQW with 6 period [sample (b)] and a 3 nm/10 nm thick $\text{In}_{0.1}\text{Ga}_{0.9}\text{N}$ MQW with 10 period [sample (c)], all of which are sandwiched between GaN layers (0.1 μm) and $\text{Al}_{0.1}\text{Ga}_{0.9}\text{N}/\text{GaN}$ (2.5 nm/2.5 nm) superlattices with 100 periods [20]. All layers are grown on GaN buffer layer and sapphire substrate by metalorganic chemical vapor deposition under undoped condition. The total active layer thickness was set to the same value as 30 nm for all samples.

In the pump-and-probe spectroscopy, the transmission spectrum of the probe beam detected in the presence of the pump beam ($T + \Delta T$) is compared to the spectrum without pump beam (T). The term of $\Delta T(E_p, I_{\text{ex}}, t_d)$ is the function of photon energy (E_p), pumping intensity (I_{ex}) and time after pulsed pump-

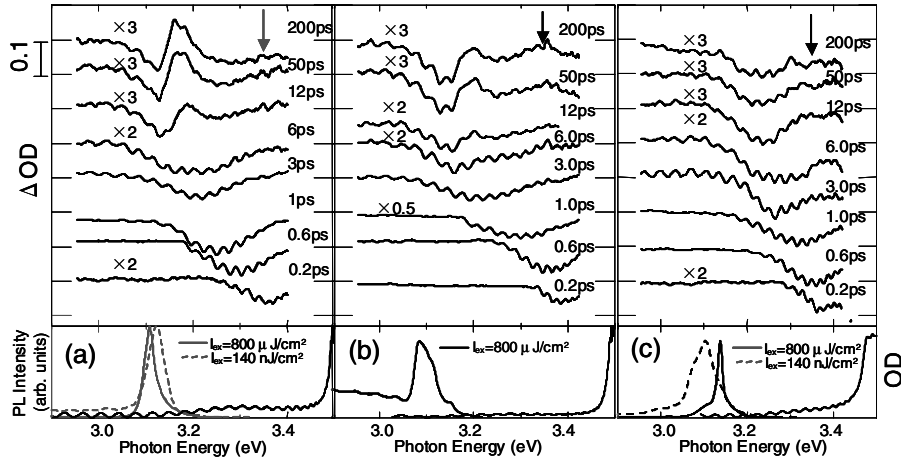


Fig. 3 ΔOD spectra of a) sample a, b) sample b and c) sample c taken at various times after pulsed excitation with photon energy of 3.350 eV (show by arrows). The OD spectra taken under Xe-lamp excitation are depicted as reference. The PL spectra are also inserted in the figure.

ing (t_d). Then the photo-induced change of the optical density [$\Delta OD(E_p, I_{ex}, t_d)$] is expressed by, $\Delta OD = \log(T/T + \Delta T) = 0.434\Delta\alpha d$, where $\Delta\alpha(E_p, I_{ex}, t_d)$ is the photo-induced change of absorption coefficient, d is the thickness of active layers [7, 8, 21, 22].

Figure 3 shows the variation of differential optical density spectra for samples a, b and c as a function of time after pumping at 370 nm (3.350 eV) under $I_{ex} = 800 \mu J/cm^2$ at 10 K. The OD spectra taken under weak-photo-excitation, as well as PL spectra are also inserted in the figure. The carrier density generated just after photo-pumping is estimated to be about $1.2 \times 10^{20} cm^{-3}$, which is well above the Mott screening density of exciton ($1 \times 10^{18} cm^{-3}$). Negative signals, peaks that make red-shift with time just after excitation, were observed in the ΔOD spectra in every sample. This is because large amount of photo-generated carriers make the band-filling of DOS leading to the gain formation, and cause the bleaching in the photo absorption. Temporal behavior of ΔOD spectra showed that photo-generated carriers rapidly reach the bottom levels in the MQWs within a time scale of several ps. For the sample a with well width (L_w) of 10 nm, negative signals in the vicinity of 3.18 eV change to positive one sandwiched between two negative peaks at 3.28 eV and 3.16 eV after a time delay more than 12 ps. For the sample b with $L_w = 5$ nm, the similar feature is observed with the sample a although the positive signals are less dominant. However, for the sample c with $L_w = 3$ nm, only negative signals were observed in the whole time range. The threshold values of I_{ex} for the stimulated emissions are about a few tens $\mu J/cm^2$ for all samples. The time-resolved PL spectroscopy revealed that the stimulated emission decays rapidly with lifetimes of less than 10 ps, and then the emission mode changes to the spontaneous one if the carrier density quenches to the lasing threshold, corresponding threshold carrier density of the order of $10^{18} cm^{-3}$ [23]. Therefore, it is probable that the carrier density is reduced to the Mott density at about 12 ps, and the excitonic absorption is restored compared to that without photo-pumping in samples a and b. These phenomena can be understood as the suppression of both Franz-Keldysh and QCSE, where electric field is screened by carriers distributed within relatively thick quantum wells. It is noted that such spectral feature is observed for the samples a and b even just after the photo-pumping if I_{ex} value is $8 \mu J/cm^2$ corresponding the initial carrier density is $1.2 \times 10^{18} cm^{-3}$. However, for the sample c, only negative signals were observed even with $I_{ex} = 8 \mu J/cm^2$, indicating that the band filling of localized states plays a more important role, and that radiative recombination takes place at the tail of absorption edge.

In order to assess the degree of potential fluctuation (spatial extent and localization depth), macroscopic PL and SNOM-PL mapping results were compared [17]. The sample for this measurement is composed of sapphire (0002) substrate, a 1.5 μm -thick undoped-GaN, a 2.3 μm -thick n-type GaN:Si, a 3nm-thick $In_xGa_{1-x}N$ -SQW ($x =$ about 0.2) [20] and a 5 nm thick undoped GaN layer. Macroscopic PL

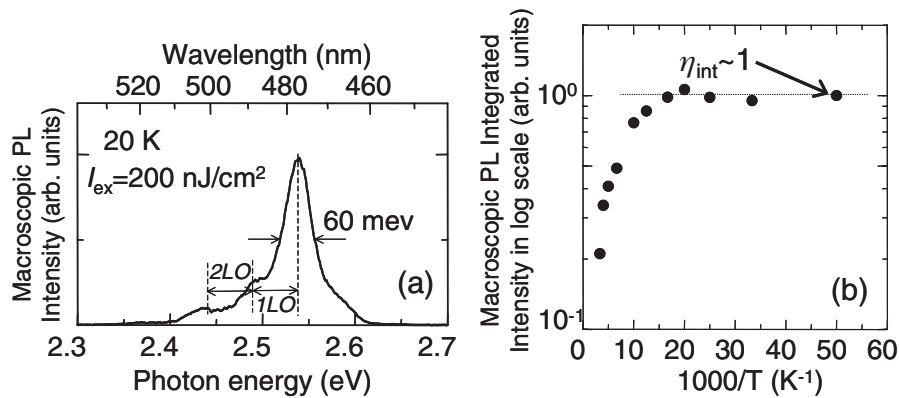


Fig. 4 a) Macroscopic PL of the sample (a 3 nm-thick $\text{In}_x\text{Ga}_{1-x}\text{N}$ -SQW) at 20 K taken with the spot size of $100 \mu\text{m} \times 100 \mu\text{m}$. b) Macroscopic integrated-PL intensity plotted as a function of inverse of temperature.

peak is located at about 480 nm associated with LO-phonon side bands at 20 K as shown in Fig. 4a. Temperature dependence of integrated PL-intensity (Fig. 4b) shows that the internal quantum efficiency is nearly unity below 50 K because of the suppression of nonradiative recombination process.

SNOM-PL measurement was performed using a 30 nm aperture probe under illumination-collection mode taken at different positions as shown in Fig. 5. Several peaks are clearly observed by using small aperture size fiber-probe and the spectral shape is different from each other. The typical PL linewidth is about 11.6 meV. This value is one fifth of macroscopic PL linewidth (about 60 meV), indicating that the macroscopic line width is not mainly contributed from the homogeneous broadening due to the interaction with phonon, but from the inhomogeneous one due to potential fluctuation. It is likely that inhomogeneous broadening due to potential fluctuations is still a significant effect on a 30 nm length scale. Therefore, even smaller PL line width might be observed with smaller aperture size.

SNOM-PL intensity mapping was performed with a 30 nm aperture under illumination collection mode as shown in Fig. 6. The images are taken with four different emission energies, ranging from low energy emission component to high energy one [(a); 2.560 eV, (b); 2.597 eV, (c); 2.615 eV and (d); 2.636 eV]. The size of island like area is in the range from 20 nm to 70 nm for (a) to (c), showing close distribution. However, islands tend to be connected if the monitored photon energy is the highest (Fig. 6d). It should be noted that such fine structures disappear if monitored under illumination mode, and that exciton/carrier localization from high-energy region to low-energy one was observed by time-resolved

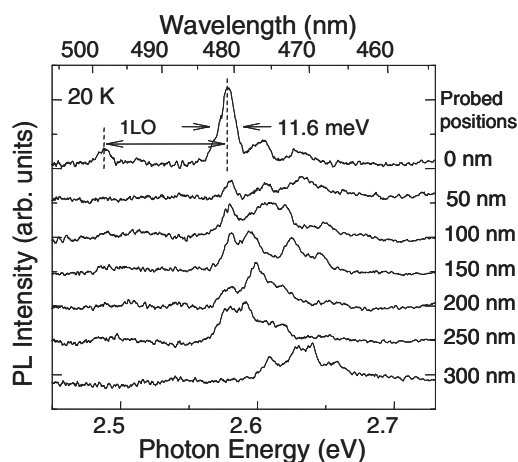


Fig. 5 SNOM-PL spectra taken at each position separated by 50 nm along one direction with a 30 nm aperture under $I_{\text{ex}} = 100 \text{ W/cm}^2$ at 20 K.

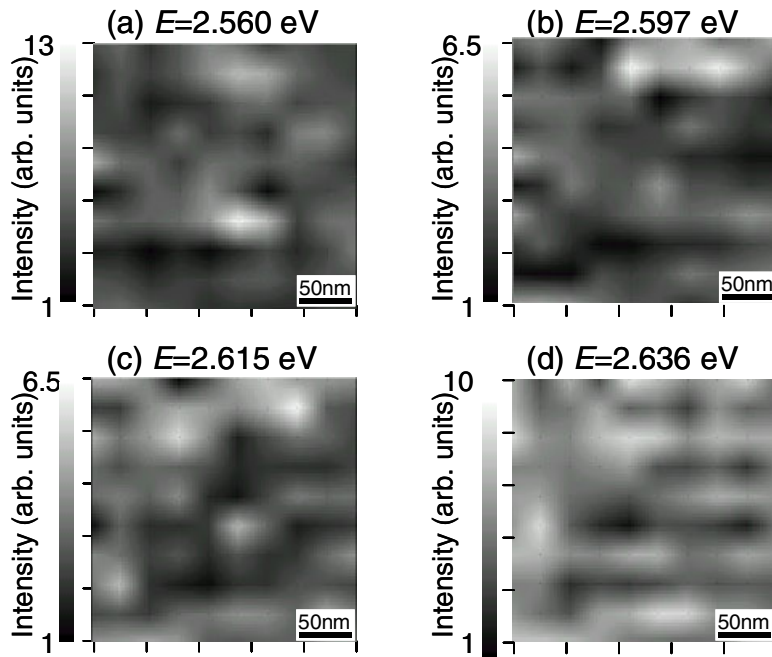


Fig. 6 SNOM-PL intensity images monitored at each emission-energy with a 30 nm aperture at 20 K.

SNOM-PL measurement [17]. Therefore, it is probable that excitons and/or carriers are deeply localized, but each localization center is so closely distributed that they are mobile within the layer. Atomic force microscopy (AFM) assessed *in-situ* during the SNOM measurements shows that the root mean square of surface unevenness is about 3 nm, and that the no correlation was found between the unevenness and PL intensity within the scanning area of 250 nm-squares. The origin of localization centers thus may be mainly due to the fluctuation of In composition rather than the interface roughness.

In conclusion, recombination dynamics has been assessed in $\text{In}_x\text{Ga}_{1-x}\text{N}$ -based quantum well structures, by employing white-light pump-and-probe spectroscopy, as well as SNOM-PL mapping. The result shows an important role of exciton/carrier localization in 3 nm-thick quantum wells.

Acknowledgements Authors would like to thank Drs. Funato and Micheletto for valuable comments and discussion. We are also grateful to Mr. Narita at JASCO corp. for contributing the set-up of SNOM. This work was partly supported by the Kyoto University VBL Project, the 21st Century COE Program (14213201) from the Japan Society for the Promotion of Science, and by a Grant-in-Aid for the special area research project of Photonics based on wavelength integration and manipulation from the Ministry of Education, Science, Sports and Culture, Japan.

References

- [1] T. Mukai, H. Narimatsu, and S. Nakamura, *Jpn. J. Appl. Phys.* **37**, L479 (1998).
- [2] T. Mukai, K. Takekawa, and S. Nakamura, *Jpn. J. Appl. Phys.* **37**, L839 (1998).
- [3] S. Nagahama, N. Iwasa, M. Senoh, T. Matsushita, Y. Sugimoto, H. Kiyoku, T. Kozaki, M. Sano, H. Matsumura, H. Umemoto, K. Chocho, and T. Mukai, *Jpn. J. Appl. Phys.* **39**, L647 (2000).
- [4] S. Nagahama, T. Yanamoto, M. Sano, and T. Mukai, *Jpn. J. Appl. Phys.* **40**, L785 (2001).
- [5] A. Shikanai, T. Deguchi, T. Sota, T. Kuroda, A. Tackeuchi, S. Chichibu, and S. Nakamura, *Appl. Phys. Lett.* **76**, 454 (2000).
- [6] K. Omae, Y. Kawakami, Sg. Fujita, M. Yamada, Y. Narukawa, and T. Mukai, *Phys. Rev. B* **65**, 077308 (2002).
- [7] K. Omae, Y. Kawakami, Y. Narukawa, Y. Watanabe, T. Mukai, and Sg. Fujita, *phys. stat. sol. (a)* **190**, 93 (2002).
- [8] Y. Narukawa, S. Saijou, Y. Kawakami, Sg. Fujita, T. Mukai, and S. Nakamura, *Appl. Phys. Lett.* **74**, 558 (1999).
- [9] S. Chichibu, T. Azuhata, T. Sota, and S. Nakamura, *Appl. Phys. Lett.* **69**, 4188 (1996).

- [10] Y. Narukawa, Y. Kawakami, M. Funato, Sg. Fujita, and S. Nakamura, Appl. Phys. Lett. **70**, 981 (1997).
- [11] Y. Narukawa, Y. Kawakami, Sz. Fujita, Sg. Fujita, and S. Nakamura, Phys. Rev. B **56**, R10024 (1997).
- [12] S. Chichibu, K. Wada, and S. Nakamura, Appl. Phys. Lett. **71**, 2346 (1997).
- [13] X. Zhang, D. H. Rich, J. T. Kobayashi, N. P. Kobayashi, and P. D. Dapkus, Appl. Phys. Lett. **73**, 1430, (1998).
- [14] T. Sugahara, M. Hao, T. Wang, D. Nakagawa, Y. Naoi, K. Nishino, and S. Sakai, Jpn. J. Appl. Phys. **37**, L1195 (1998).
- [15] P. A. Crowell, D. K. Young, S. Keller, E. L. Hu, and D. D. Awschalom, Appl. Phys. Lett. **72**, 927 (1998).
- [16] A. Vertikov, M. Kuball, A. V. Nurmikko, Y. Chen, and S.-Y. Wang, Appl. Phys. Lett. **72**, 2645 (1998).
- [17] A. Kaneta, K. Okamoto, Y. Kawakami, Sg. Fujita, G. Marutsuki, Y. Narukawa, and T. Mukai, Appl. Phys. Lett. **81**, 4353 (2002).
- [18] G. Marutsuki, Y. Narukawa, T. Mitani, T. Mukai, G. Shinomiya, A. Kaneta, Y. Kawakami, and Sg. Fujita, phys. stat. sol. (a) **192**, 100 (2002).
- [19] T. Saiki, K. Nishi, and M. Ohtsu, Jpn. J. Appl. Phys. **37**, 1638 (1998).
- [20] It should be noted that In compositions estimated by growth conditions may be overestimated considering recent-reported values of InN bandgap energy (0.7–0.8 eV) and bowing parameter of $\text{In}_x\text{Ga}_{1-x}\text{N}$ ($b = 2.3$ eV).
- [21] Y. Kawakami, Y. Narukawa, K. Omae, S. Nakamura, and Sg. Fujita, Mater. Sci. Eng. B **82**, 188 (2001).
- [22] Y. Kawakami, Y. Narukawa, K. Omae, S. Nakamura, and Sg. Fujita, Appl. Phys. Lett. **77**, 2151 (2000).
- [23] Y. Narukawa, Y. Kawakami, Sg. Fujita, and S. Nakamura, phys. stat. sol. (b) **176**, 39 (1999).